Spontaneous Oxygen Vacancy Ionization Enhances Water Oxidation on BiVO<inf>4</inf>

ACS Energy LETTERS

http://pubs.acs.org/journal/aelccp

LETTER

Spontaneous Oxygen Vacancy Ionization Enhances Water Oxidation on $BiVO_4$

Nicklas Österbacka, Hassan Ouhbi, Francesco Ambrosio, and Julia Wiktor*

Cite This: *ACS Energy Lett.* 2024, 9, 153−158

Read Online

ACCESS | Metrics & More | Article Recommendations | Supporting Information

ABSTRACT: The influence of surface oxygen vacancies on the oxygen evolution reaction on bismuth vanadate is studied using hybrid density functional theory. Our findings reveal that the neutral charge state is thermodynamically unfavorable, leading to spontaneous ionization of V_O^0 into V_O^{2+}. By investigating the oxygen evolution reaction mechanism on both stoichiometric and oxygen-deficient surfaces, we find that surface oxygen vacancies reduce the reaction's thermodynamic overpotential but only when the defects are ionized. Moreover, the reaction pathway involves the formation of surface-bound peroxide and superoxide ions as intermediates. Our work provides insight into the nature of surface oxygen vacancies and shines new light on how they may enhance the photoelectrochemical properties of semiconductors.

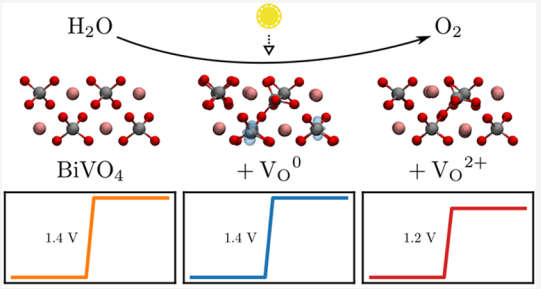

Solar water splitting offers an attractive pathway toward clean energy, enabling the production of hydrogen gas from nothing but water and solar light. The process consists of two halves: the cathodic hydrogen evolution reaction and the anodic oxygen evolution reaction (OER). The latter involves four proton-coupled electron transfers and thus requires a photoanode with excellent charge transfer properties to overcome its sluggish kinetics.[1] While a great deal of research has been put into improving the anode, the OER remains the bottleneck in the overall water splitting process.[1−3]

The ideal OER (photo)catalyst should be cheap and stable and exhibit a moderate bandgap that allows for light absorption in the visible regime to maximize efficiency.[1,4] On paper, monoclinic bismuth vanadate ($BiVO_4$), an n-type semiconductor with a bandgap of 2.4 eV, fulfills these requirements.[5] However, the practical photoelectrochemical (PEC) performance of the material is limited by high charge recombination rates, low conductivity, and slow charge transfer rates. Several strategies for improving upon these shortcomings have been developed in recent years, including cocatalyst deposition and doping.[6−9] Intrinsic defects also significantly alter the properties of the host material, with several studies suggesting that an abundance of oxygen vacancies (V_O) improves the PEC performance of $BiVO_4$.[10−14] The defect could also play a more direct role in the reaction as proposed by Hermans et al.[15] and explored computationally by Nikačević et al.[16] A complete and coherent picture of the mechanism behind the improvement is still missing, however.

Additionally, the nature of surface polarons in water adsorption and reactivity on $BiVO_4$ has been elucidated in recent studies. The work of Wang et al.[17] demonstrated how surface polarons facilitate water splitting, while that of Steinitz-Eliyahu et al.[18] explored the interplay between surface polarons and defect states. These insights into the role of surface polarons further enrich our understanding of defect-mediated processes on $BiVO_4$ surfaces, providing a broader context for our investigation into the influence of surface oxygen vacancies on the oxygen evolution reaction in $BiVO_4$. This nuanced understanding of various defect states, including both oxygen vacancies and surface polarons, sets the stage for a more comprehensive exploration of the electrochemistry of $BiVO_4$, which is the focus of the present study.

In this work, we investigate the stability of the surface V_O in $BiVO_4$ in different charge states and find that it spontaneously ionizes. We furthermore calculate how the thermodynamic overpotential of the oxygen evolution reaction is affected by the presence of V_O at the surface. In the neutral charge state, they have no effect on this property, while ionized vacancies (V_O^{2+}) reduce the overpotential by 0.2 V. Additionally, the proposed reaction pathway involves formation of surface-bound perodixe and superoxide species.

Defect formation energies are computed within the framework laid out by Freysoldt and Neugebauer for charged

Received: November 2, 2023
Revised: December 5, 2023
Accepted: December 7, 2023
Published: December 13, 2023

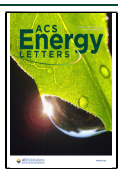

defects at surfaces.[19] Total energies are evaluated with a PBE0-based density functional with 22% exact exchange, which reproduces the QSGŴ bandgap and is expected to give a correct description of polaronic distortions,[20,21] as implemented in CP2K.[22] A more detailed overview of the computational methodology is given in Section S1 of the Supporting Information, where we also show that the defect formation energies are insensitive to the computational setup (Figures S1, S2, and S3). For simplicity, we consider the (001) surface of $I4_1/a$ tetragonal scheelite $BiVO_4$ with cell parameters ($a = b = 5.147$ Å, $c = 11.726$ Å) in agreement with the experimental findings of Sleight et al.[23] instead of the (001) surface of the $I2/b$ monoclinic scheelite form as the electronic properties differ little between the two surfaces.[24] We note that the latter is equivalent to the (010) surface of the $C2/c$ representation. $2 \times 2 \times 2$ repetitions of the ideal structure with 30 Å of vacuum in the surface normal direction are used to approximate the surface. When considering reaction free energies, the bottom two layers of the slabs are frozen to the geometry of the optimized bulk and a dipole correction is applied for the charge-neutral systems. An extrapolation scheme is used to get size-converged free energy differences for the ionized oxygen-deficient surface as outlined in Section S4 of the Supporting Information, along with the results of the procedure (Figure S5).

The OER mechanism typically considered in mechanistic studies consists of four steps, each involving the transfer of a proton−electron pair:

$$
\begin{aligned}
&1.\quad * + H_2O \rightarrow {}^*OH + (H^+ + e^-)\\
&2.\quad {}^*OH \rightarrow {}^*O + (H^+ + e^-)\\
&3.\quad {}^*O + H_2O \rightarrow {}^*OOH + (H^+ + e^-)\\
&4.\quad {}^*OOH \rightarrow * + (H^+ + e^-) + O_2
\end{aligned}
\qquad (1)
$$

Here, a lone $*$ denotes the bare surface, while *X denotes adsorption of X. The free energy difference at pH 0 of each reaction step is evaluated within the computational hydrogen electrode (CHE) formalism.[25] Details of the vibrational analysis may be found in Section S4 of the Supporting Information, along with an illustration of the included atoms (Figure S4), as well as tables of the vibrational frequencies (Tables S1 and S2) and the resulting free energy components (Tables S3 and S4). The oxygen molecule is notoriously difficult to describe using density functional theory (DFT), so the free energy of the total reaction, i.e., $2H_2O \rightarrow O_2 + 4(H^+ + e^-)$, is set to the experimental value of 4.96 eV. In the following, we report only the lowest-energy pathway for each surface.

Removing an oxygen atom from the surface of $BiVO_4$ leads to a significant distortion of the lattice. The vanadium atom closest to the vacancy is pushed into the surface, sharing an oxygen atom with a subsurface VO_4 to retain its 4-fold coordination as shown in Figure S4. The introduction of the oxygen vacancy additionally frees two excess electrons, which may localize at different sites in the lattice. In the stablest configuration, one electron localizes onto the corner-sharing V below the vacancy and the other at a nearby subsurface V site. We additionally find this structure to be non-spin-polarized, as the triplet spin state is 5 meV higher in energy than the singlet. It may be energetically favorable for the vacancy to be ionized instead, however. We investigate this by computing defect formation energies, shown in Figure 1. Here, the chemical potential of oxygen is fixed to values corresponding to the oxygen-rich limit in our previous work.[26] The formation energy of V_O^{1+} is higher than the other charge states across the entire Fermi level range, and the charge state is thus thermodynamically unfavorable. Also shown is the charge transition level (CTL) of the electron polaron in the subsurface, which is the preferred localization site for excess electrons in stoichiometric $BiVO_4$. The (+2/0) CTL lies 0.4 eV above that of the polaron, indicating that it is energetically favorable for the excess electrons stemming from the vacancy to form small polarons in stoichiometric regions of the material rather than occupying states associated with the oxygen vacancies. In other words, the vacancy should spontaneously ionize and thus predominantly be in the ionized +2 charge state.

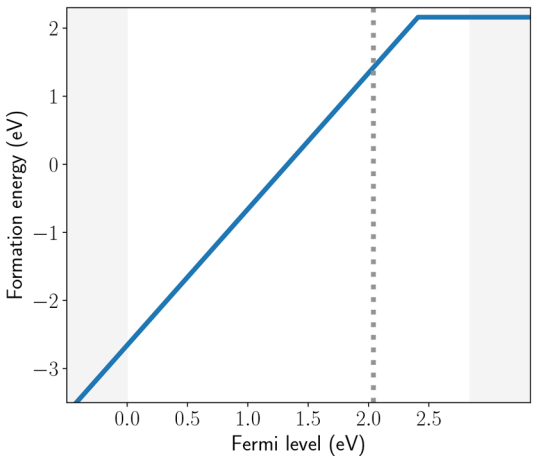

Figure 1. Formation energy for the surface oxygen vacancy in $BiVO_4$. The dashed vertical line indicates the CTL of the electron polaron in defect-free $BiVO_4$. The valence and conduction bands are shown in gray.

The effect of V_O formation and ionization on the OER mechanism is investigated by finding the stablest intermediates for the OER, taking only the steps involving proton-coupled electron transfer into account. Renders of the resulting pathways for the reaction on the stoichiometric as well as the neutral (0) and ionized (2+) oxygen-deficient surfaces are shown in Figure 2. The free energy profiles of each reaction pathway, calculated within the CHE formalism, are shown in Figure 3. This allows us to compare the efficiency of the mechanisms by computing their thermodynamic overpotentials. This is determined by the difference between the highest free energy difference of each reaction profile, i.e., the potential-determining step (PDS) and the ideal free energy cost of 1.23 eV.

The primary active site on the stoichiometric surface is a bismuth atom. The PDS is the very first step, ending up with an OH group adsorbed onto a surface bismuth site, with an overpotential of 1.4 V. The second reaction step results in the formation of an oxygen dimer with an O−O bond length of 1.45 Å. With the neutral vacancy, the reaction instead proceeds by filling the vacancy. The stoichiometric surface is recovered after the second reaction step, highlighted by the shared intermediates in Figure 2. The PDS is the third step, resulting in a Bi-adsorbed OH group and an overpotential of 1.4 V. In other words, the PDS is the same for both of these cases, as illustrated in Figure 2. The fourth step of the latter reaction

https://doi.org/10.1021/acsenergylett.3c02348
ACS Energy Lett. 2024, 9, 153−158

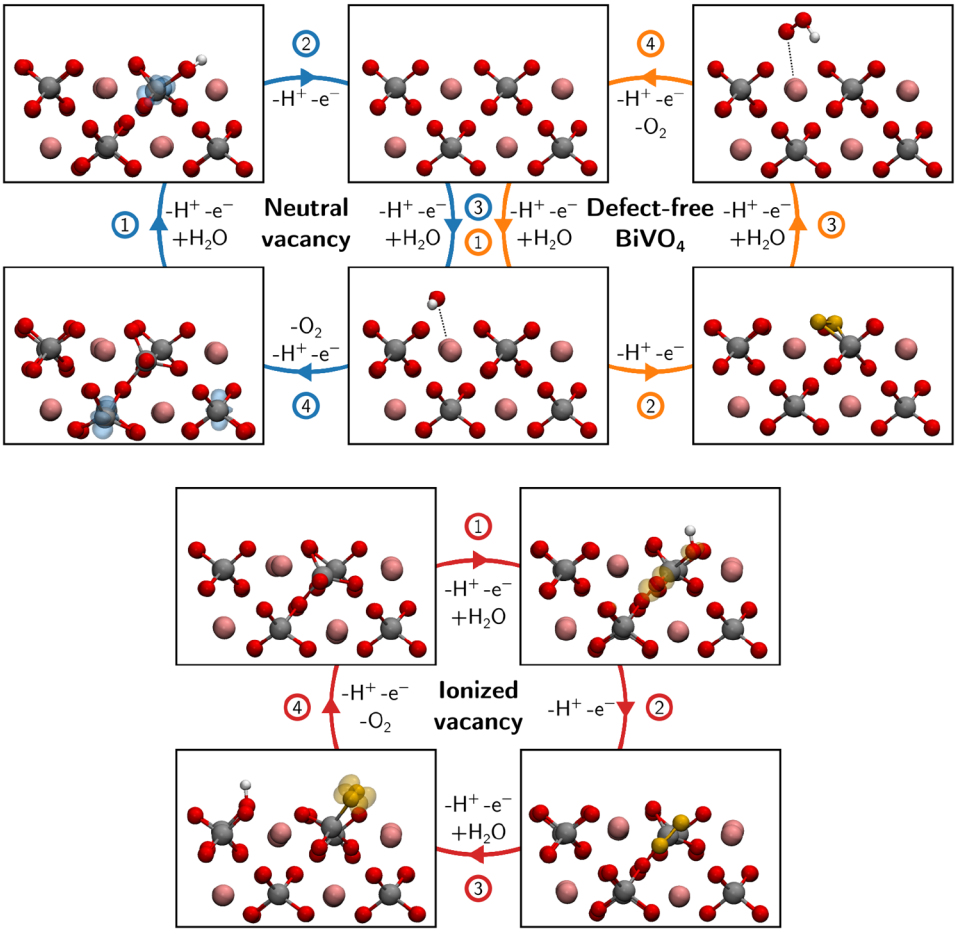

Figure 2. Schematic illustration of the OER reaction mechanism showing side views of the surface structure of each intermediate. The inset numbers correspond to the reaction step numbering in eq 1. Isosurfaces correspond to localized charges, with electrons colored blue and holes yellow. Oxygen atoms involved in dimerization are colored yellow. The dotted lines highlight the Bi−O bond formed with the adsorbed OH and OOH in some reaction steps.

reintroduces the V_O, resulting in a higher free energy cost than the corresponding (third) step on the stoichiometric surface, involving only a proton−electron pair.

On the surface with V_O^{2+}, the vacancy is the active site. The PDS is the first step, with an overpotential of 1.2 V, resulting in an OH group filling the V_O. As the positive charge state is fixed throughout the entire reaction, an excess hole is localized in close vicinity of the adsorbate. The second reaction step yields the stoichiometric structure but with two excess holes. These localize onto two surface oxygen atoms, resulting in the formation of an oxygen dimer, or a peroxide ion (O_2^{2-}), with an O−O bond bond length of 1.45 Å. After the third reaction step, yet another excess hole localizes onto the adsorbed dimer, resulting in a surface-bound superoxide ion (O_2^{1-}) with O−O bond length 1.32 Å. We note that the surface-bound O_2^{2-} exhibits no spin polarization and the O_2^{1-} has a lone unpaired electron. Alternative, higher-energy, adsorption modes for the *OOH intermediate are shown in Figure S6. After the removal of the final hydrogen atom, an oxygen molecule is evolved and the vacancy reintroduced at a significantly lower free energy cost than in the un-ionized case.

The formation energy of V_O^0 is greater than that of V_O^{2+} plus two electron polarons, as may be seen in Figure 1, indicating that the defect spontaneously ionizes no matter the Fermi level. It is always energetically favorable for the excess electrons stemming from the vacancy to localize in stoichiometric regions of the material, neglecting potential interactions with other defects. This is in agreement with the revised results of Wang et al.[27,28] Experiments by Selim et al. indicate that ionized V_O are dominant also at the semiconductor/electrolyte interface of experimentally realized $BiVO_4$-based photoanodes in the dark.[29]

The spontaneous ionization of surface V_O into V_O^{2+} additionally implies that they do not act as hole trapping sites unlike neutral V_O^0, in agreement with the calculations of Cheng et al.[30] This increases the number of photogenerated holes that are able to participate in the OER. Furthermore, the concentration of V_O is not measured directly in experiments. Instead, the concentration of near-surface paramagnetic V^{4+} is probed through electron spin resonance.[29,31] These paramagnetic centers arise from the localization of excess electrons stemming from vacancy formation, reducing V^{5+} in the surface region. The spontaneous ionization of surface V_O implies that the elevation in V^{4+} concentration associated with oxygen vacancy enrichment stems from subsurface polarons rather than states directly associated with the defects themselves. The energy landscape of intrinsic defects in $BiVO_4$ is complex,[26,32] and disentangling oxygen vacancy-related V^{4+} to those stemming from other intrinsic donor defects would be nigh impossible. The 2:1 V^{4+}−V_O relationship assumed when

https://doi.org/10.1021/acsenergylett.3c02348
ACS Energy Lett. 2024, 9, 153−158

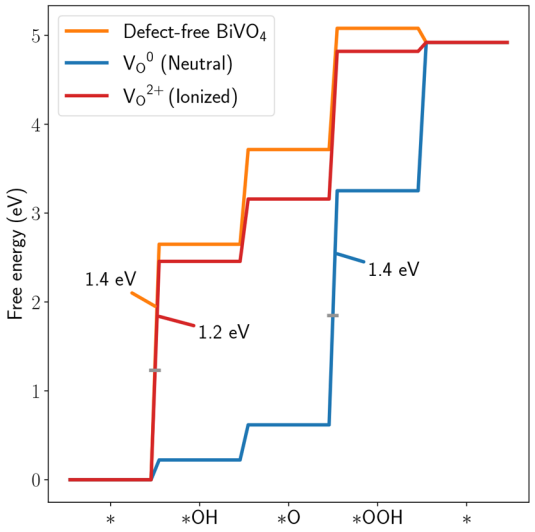

Figure 3. Free energy profiles for the OER as shown in eq 1 on stoichiometric as well as oxygen-deficient $BiVO_4$, with the latter shown in both neutral (0) and ionized (+2) charge states. The location of the ideal barrier height for each PDS is marked with a horizontal bar, and the excess barrier energy is also shown. These result in overpotentials of 1.4 V for the stoichiometric surface, 1.4 V for V_O^0, and 1.2 V for the ionized V_O^{2+}.

reporting oxygen vacancy concentrations in the literature may thus be flawed, though more detailed studies should be conducted to clarify this.

The optimal, i.e., lowest-energy, reaction pathways outlined in Figure 2 for the stoichiometric and the neutral oxygen-deficient surfaces agree well with mechanisms previously considered in the literature.[16,33] The two mechanisms share two intermediates. Once they reach the step corresponding to OH adsorption onto the stoichiometric structure, the reaction may proceed either through removal of proton−electron pair or through the removal of both a proton−electron pair and an oxygen molecule. The latter process reintroduces the vacancy, and the pathway involving surface V_O^0 is thus equivalent to starting from the stoichiometric structure and removing a lattice oxygen atom during one step of the reaction. OER pathways that directly involve lattice oxygen have been proposed for several metal oxides,[34−38] including bismuth vanadate,[15] but our results suggest that the mechanism fails to increase the OER activity in comparison to that of stoichiometric $BiVO_4$.

Nikačević et al. propose an alternative reaction mechanism on the neutral oxygen-deficient surface, where the intermediates adsorb onto a surface bismuth atom next to the defect instead of filling the vacancy.[16] They found that this scheme results in a lower overpotential but also estimate that around 97% of the surface vacancies would be filled at room temperature based on energy differences. We find that filling the vacancy is energetically favorable for each step of the reaction and the reactant can thus enter the vacancy at any point (Table S5). We thus deem that it is unlikely for this alternative mechanism to be the primary driving force behind the OER activity of $BiVO_4$ and exclude it from this study.

On the surface with V_O^{2+}, the OER proceeds through filling and subsequent reintroduction of the vacancy in a fashion similar to the mechanism involving V_O^0. This process is associated with a significantly lower energy cost for the ionized surface, however, which also exhibits a thermodynamic overpotential that is 0.2 V lower than the other cases considered here. The reaction thus becomes more favorable upon vacancy ionization. The mechanism we propose involves the formation of surface-bound peroxide and superoxide ions. Wang et al. have proposed a similar mechanism for the OER on TiO_2,[3] and the surface-bound peroxide ion on $BiVO_4$ has been predicted to be stable even in the presence of water by Wiktor and Ambrosio.[20] The last OER step consists of the reaction $O_2^{1-} + h^+ \rightarrow O_2$. This can be expected to occur quickly upon superoxide generation, as the standard reduction potential for the O_2/O_2^{1-} redox couple lies around 0.33 V above the conduction band minimum of $BiVO_4$,[39] thus allowing for rapid hole injection to drive the reaction. As a consequence, the lifetime of the superoxide intermediate is likely short.

As highlighted by our results as well as by Todorova and Neugebauer,[40] the effect of defects on the electrochemical properties of a material depends on their charge state. As outlined above, our results indicate that the fully ionized V_O is dominant in $BiVO_4$ no matter the Fermi level. This need not be the case for other OER photoanode materials, however. This opens up the possibility of tailoring photoanode properties through Fermi level engineering by carefully controlling defect and dopant concentrations as has previously been done for the NV center in diamond and $BaZrO_3$ multilayer structures.[41,42]

The intertwining roles of oxygen vacancies and surface polarons, as laid out in our study and those by Wang et al.[17] and Steinitz-Eliyahu et al.,[18] open avenues for a more holistic approach in defect engineering. The collective understanding allows for a nuanced exploration of defect-controlled electrochemical properties, fostering the advancement of photoanode materials for efficient solar water splitting.

In conclusion, we find that surface oxygen vacancies in $BiVO_4$ spontaneously ionize and therefore do not act as hole traps unlike un-ionized vacancies. Computational investigation of the oxygen evolution reaction intermediates shows that this ionization enables a reaction pathway that exhibits a lower thermodynamic overpotential than the optimal pathways on stoichiometric and un-ionized oxygen-deficient surfaces. Enriching the surface of $BiVO_4$ thus makes the oxygen evolution reaction more favorable and improves the majority carrier concentration while allowing for more photoexcited holes to partake in the reaction. The reaction intermediates in the pathway we propose on the ionized oxygen-deficient surface involve the formation of surface-bound peroxide (O_2^{2-}) and superoxide (O_2^{1-}) ions. We argue that the superoxide intermediate is very short-lived, allowing for rapid formation of oxygen molecules and the reintroduction of the vacancy to the surface. Our results shine new light on the nature of surface oxygen vacancies in $BiVO_4$ and the manner in which they improve the photoelectrochemical activity as observed experimentally in oxygen-deficient samples of the material. They also highlight the importance of taking the full picture of defect and dopant occupancy into account when considering reactions involving nonstoichiometric surfaces.

■ ASSOCIATED CONTENT

Supporting Information

The Supporting Information is available free of charge at https://pubs.acs.org/doi/10.1021/acsenergylett.3c02348.

https://doi.org/10.1021/acsenergylett.3c02348
ACS Energy Lett. 2024, 9, 153−158

Details of computational methodology, defect formation energies with different values of the dielectric constant, defect formation energies with different fraction of exact exchange and with DFT+U, details of vibrational analysis with tables of vibrational frequencies and free energy components, alternative adsorption modes for *OOH on the surface with V_O^{2+}, and a discussion on alternative pathways for the oxygen evolution reaction on the neutral oxygen-deficient surface (PDF)

AUTHOR INFORMATION

Corresponding Author

Julia Wiktor − *Department of Physics, Chalmers University of Technology, SE-412 96 Gothenburg, Sweden;* orcid.org/0000-0003-3395-1104; Email: julia.wiktor@chalmers.se

Authors

Nicklas Österbacka − *Department of Physics, Chalmers University of Technology, SE-412 96 Gothenburg, Sweden;* orcid.org/0000-0002-6043-4607

Hassan Ouhbi − *Department of Physics, Chalmers University of Technology, SE-412 96 Gothenburg, Sweden;* orcid.org/0000-0001-7371-4782

Francesco Ambrosio − *Dipartimento di Scienze, Università degli Studi della Basilicata, 10-85100 Potenza, Italy; Dipartimento di Chimica e Biologia Adolfo Zambelli, Università di Salerno, I-84084 Fisciano, SA, Italy;* orcid.org/0000-0002-6388-9586

Complete contact information is available at: https://pubs.acs.org/10.1021/acsenergylett.3c02348

Notes

The authors declare no competing financial interest.

ACKNOWLEDGMENTS

The authors acknowledge funding from the "Area of Advance-Materials Science" at Chalmers University of Technology and from the Swedish Research Council (Grant 2019-03993). The computations were performed on resources provided by the National Academic Infrastructure for Supercomputing in Sweden (NAISS) at NSC and PDC. The authors thank Christoph Freysoldt and Hannu-Pekka Komsa for their helpful input on finite-size corrections. F.A. thankfully acknowledges the PRIN-PNRR 2022 project DELPHI (project code: P2022W9773).

REFERENCES

(1) Song, J.; Wei, C.; Huang, Z.-F.; Liu, C.; Zeng, L.; Wang, X.; Xu, Z. J. A Review on Fundamentals for Designing Oxygen Evolution Electrocatalysts. *Chem. Soc. Rev.* **2020**, *49*, 2196−2214.

(2) Fabbri, E.; Schmidt, T. J. Oxygen Evolution Reaction—The Enigma in Water Electrolysis. *ACS Catal.* **2018**, *8*, 9765−9774.

(3) Wang, D.; Sheng, T.; Chen, J.; Wang, H.-F.; Hu, P. Identifying the Key Obstacle in Photocatalytic Oxygen Evolution on Rutile TiO_2. *Nat. Catal* **2018**, *1*, 291−299.

(4) Jiang, C.; Moniz, S. J. A.; Wang, A.; Zhang, T.; Tang, J. Photoelectrochemical Devices for Solar Water Splitting − Materials and Challenges. *Chem. Soc. Rev.* **2017**, *46*, 4645−4660.

(5) Park, Y.; McDonald, K. J.; Choi, K.-S. Progress in Bismuth Vanadate Photoanodes for Use in Solar Water Oxidation. *Chem. Soc. Rev.* **2013**, *42*, 2321−2337.

(6) Abdi, F. F.; Firet, N.; van de Krol, R. Efficient $BiVO_4$ Thin Film Photoanodes Modified with Cobalt Phosphate Catalyst and W-doping. *ChemCatChem* **2013**, *5*, 490−496.

(7) Zhang, B.; Zhang, H.; Wang, Z.; Zhang, X.; Qin, X.; Dai, Y.; Liu, Y.; Wang, P.; Li, Y.; Huang, B. Doping Strategy to Promote the Charge Separation in $BiVO_4$ Photoanodes. *Appl. Catal., B* **2017**, *211*, 258−265.

(8) Palaniselvam, T.; Shi, L.; Mettela, G.; Anjum, D. H.; Li, R.; Katuri, K. P.; Saikaly, P. E.; Wang, P. Vastly Enhanced $BiVO_4$ Photocatalytic OER Performance by $NiCoO_2$ as Cocatalyst. *Adv. Mater. Interfaces* **2017**, *4*, 1700540.

(9) Talasila, G.; Sachdev, S.; Srivastva, U.; Saxena, D.; Ramakumar, S. S. V. Modified Synthesis of $BiVO_4$ and Effect of Doping (Mo or W) on Its Photoelectrochemical Performance for Water Splitting. *Energy Reports* **2020**, *6*, 1963−1972.

(10) Feng, S.; Wang, T.; Liu, B.; Hu, C.; Li, L.; Zhao, Z.-J.; Gong, J. Enriched Surface Oxygen Vacancies of Photoanodes by Photoetching with Enhanced Charge Separation. *Angew. Chem., Int. Ed.* **2020**, *59*, 2044−2048.

(11) Wu, J.-M.; Chen, Y.; Pan, L.; Wang, P.; Cui, Y.; Kong, D.; Wang, L.; Zhang, X.; Zou, J.-J. Multi-Layer Monoclinic $BiVO_4$ with Oxygen Vacancies and V^{4+} Species for Highly Efficient Visible-Light Photoelectrochemical Applications. *Appl. Catal., B* **2018**, *221*, 187−195.

(12) Jin, S.; Ma, X.; Pan, J.; Zhu, C.; Saji, S. E.; Hu, J.; Xu, X.; Sun, L.; Yin, Z. Oxygen Vacancies Activating Surface Reactivity to Favor Charge Separation and Transfer in Nanoporous $BiVO_4$ Photoanodes. *Appl. Catal. B: Environmental* **2021**, *281*, 119477.

(13) Wang, S.; Chen, P.; Bai, Y.; Yun, J.-H.; Liu, G.; Wang, L. New $BiVO_4$ Dual Photoanodes with Enriched Oxygen Vacancies for Efficient Solar-Driven Water Splitting. *Adv. Mater.* **2018**, *30*, 1800486.

(14) Wang, S.; He, T.; Chen, P.; Du, A.; Ostrikov, K. K.; Huang, W.; Wang, L. In Situ Formation of Oxygen Vacancies Achieving Near-Complete Charge Separation in Planar $BiVO_4$ Photoanodes. *Adv. Mater.* **2020**, *32*, 2001385.

(15) Hermans, Y.; Murcia-López, S.; Klein, A.; Jaegermann, W. $BiVO_4$ Surface Reduction upon Water Exposure. *ACS Energy Lett.* **2019**, *4*, 2522−2528.

(16) Nikačević, P.; Hegner, F. S.; Galán-Mascarós, J. R.; López, N. Influence of Oxygen Vacancies and Surface Facets on Water Oxidation Selectivity toward Oxygen or Hydrogen Peroxide with $BiVO_4$. *ACS Catal.* **2021**, *11*, 13416−13422.

(17) Wang, W.; Favaro, M.; Chen, E.; Trotochaud, L.; Bluhm, H.; Choi, K.-S.; van de Krol, R.; Starr, D. E.; Galli, G. Influence of Excess Charge on Water Adsorption on the $BiVO_4$(010) Surface. *J. Am. Chem. Soc.* **2022**, *144*, 17173−17185.

(18) Steinitz-Eliyahu, R.; Hernangómez-Pérez, D.; Hegner, F. S.; Nikačević, P.; López, N.; Refaely-Abramson, S. Mixed Excitonic Nature in Water-Oxidized $BiVO_4$ Surfaces with Defects. *Phys. Rev. Materials* **2022**, *6*, 065402.

(19) Freysoldt, C.; Neugebauer, J. First-Principles Calculations for Charged Defects at Surfaces, Interfaces, and Two-Dimensional Materials in the Presence of Electric Fields. *Phys. Rev. B* **2018**, *97*, 205425.

(20) Ambrosio, F.; Wiktor, J. Strong Hole Trapping Due to Oxygen Dimers in $BiVO_4$: Effect on the Water Oxidation Reaction. *J. Phys. Chem. Lett.* **2019**, *10*, 7113−7118.

(21) Chen, W.; Miceli, G.; Rignanese, G.-M.; Pasquarello, A. Nonempirical Dielectric-Dependent Hybrid Functional with Range Separation for Semiconductors and Insulators. *Phys. Rev. Mater.* **2018**, *2*, 073803.

(22) Kühne, T. D.; et al. CP2K: An Electronic Structure and Molecular Dynamics Software Package - Quickstep: Efficient and Accurate Electronic Structure Calculations. *J. Chem. Phys.* **2020**, *152*, 194103.

(23) Sleight, A. W.; Chen, H. y.; Ferretti, A.; Cox, D. E. Crystal Growth and Structure of $BiVO_4$. *Mater. Res. Bull.* **1979**, *14*, 1571−1581.

(24) Lee, D.; Wang, W.; Zhou, C.; Tong, X.; Liu, M.; Galli, G.; Choi, K.-S. The Impact of Surface Composition on the Interfacial Energetics and Photoelectrochemical Properties of $BiVO_4$. *Nat. Energy* **2021**, *6*, 287.

(25) Nørskov, J. K.; Rossmeisl, J.; Logadottir, A.; Lindqvist, L.; Kitchin, J. R.; Bligaard, T.; Jónsson, H. Origin of the Overpotential for Oxygen Reduction at a Fuel-Cell Cathode. *J. Phys. Chem. B* **2004**, *108*, 17886−17892.
(26) Österbacka, N.; Ambrosio, F.; Wiktor, J. Charge Localization in Defective $BiVO_4$. *J. Phys. Chem. C* **2022**, *126*, 2960−2970.
(27) Wang, W.; Strohbeen, P. J.; Lee, D.; Zhou, C.; Kawasaki, J. K.; Choi, K.-S.; Liu, M.; Galli, G. The Role of Surface Oxygen Vacancies in $BiVO_4$. *Chem. Mater.* **2020**, *32*, 2899−2909.
(28) Wang, W.; Strohbeen, P. J.; Lee, D.; Zhou, C.; Kawasaki, J. K.; Choi, K.-S.; Liu, M.; Galli, G. Correction: The Role of Surface Oxygen Vacancies in $BiVO_4$. *Chem. Mater.* **2023**, *35*, 8321−8322.
(29) Selim, S.; Pastor, E.; García-Tecedor, M.; Morris, M. R.; Francàs, L.; Sachs, M.; Moss, B.; Corby, S.; Mesa, C. A.; Gimenez, S.; Kafizas, A.; Bakulin, A. A.; Durrant, J. R. Impact of Oxygen Vacancy Occupancy on Charge Carrier Dynamics in $BiVO_4$ Photoanodes. *J. Am. Chem. Soc.* **2019**, *141*, 18791−18798.
(30) Cheng, C.; Fang, Q.; Fernandez-Alberti, S.; Long, R. Controlling Charge Carrier Trapping and Recombination in $BiVO_4$ with the Oxygen Vacancy Oxidation State. *J. Phys. Chem. Lett.* **2021**, *12*, 3514−3521.
(31) Tan, H. L.; Suyanto, A.; Denko, A. T. D.; Saputera, W. H.; Amal, R.; Osterloh, F. E.; Ng, Y. H. Enhancing the Photoactivity of Faceted $BiVO_4$ via Annealing in Oxygen-Deficient Condition. *Part. Part. Syst. Charact.* **2017**, *34*, 1600290.
(32) Zhang, J.; Chen, X.; Deng, M.; Shen, H.; Li, H.; Ding, J. Effects of Native Defects and Cerium Impurity on the Monoclinic $BiVO_4$ Photocatalyst Obtained *via* PBE+*U* Calculations. *Phys. Chem. Chem. Phys.* **2020**, *22*, 25297−25305.
(33) Hu, J.; Chen, W.; Zhao, X.; Su, H.; Chen, Z. Anisotropic Electronic Characteristics, Adsorption, and Stability of Low-Index $BiVO_4$ Surfaces for Photoelectrochemical Applications. *ACS Appl. Mater. Interfaces* **2018**, *10*, 5475−5484.
(34) Binninger, T.; Mohamed, R.; Waltar, K.; Fabbri, E.; Levecque, P.; Kötz, R.; Schmidt, T. J. Thermodynamic Explanation of the Universal Correlation between Oxygen Evolution Activity and Corrosion of Oxide Catalysts. *Sci. Rep.* **2015**, *5*, 12167.
(35) Mefford, J. T.; Rong, X.; Abakumov, A. M.; Hardin, W. G.; Dai, S.; Kolpak, A. M.; Johnston, K. P.; Stevenson, K. J. Water Electrolysis on $La_{1-x}Sr_xCoO_{3-\delta}$ Perovskite Electrocatalysts. *Nat. Commun.* **2016**, *7*, 11053.
(36) Grimaud, A.; Diaz-Morales, O.; Han, B.; Hong, W. T.; Lee, Y.-L.; Giordano, L.; Stoerzinger, K. A.; Koper, M. T. M.; Shao-Horn, Y. Activating Lattice Oxygen Redox Reactions in Metal Oxides to Catalyse Oxygen Evolution. *Nat. Chem.* **2017**, *9*, 457−465.
(37) Yoo, J. S.; Rong, X.; Liu, Y.; Kolpak, A. M. Role of Lattice Oxygen Participation in Understanding Trends in the Oxygen Evolution Reaction on Perovskites. *ACS Catal.* **2018**, *8*, 4628−4636.
(38) Zagalskaya, A.; Evazzade, I.; Alexandrov, V. Ab Initio Thermodynamics and Kinetics of the Lattice Oxygen Evolution Reaction in Iridium Oxides. *ACS Energy Lett.* **2021**, *6*, 1124−1133.
(39) Monfort, O.; Plesch, G. Bismuth Vanadate-Based Semiconductor Photocatalysts: A Short Critical Review on the Efficiency and the Mechanism of Photodegradation of Organic Pollutants. *Environ. Sci. Pollut Res.* **2018**, *25*, 19362−19379.
(40) Todorova, M.; Neugebauer, J. Identification of Bulk Oxide Defects in an Electrochemical Environment. *Faraday Discuss.* **2015**, *180*, 97−112.
(41) Murai, T.; Makino, T.; Kato, H.; Shimizu, M.; Murooka, T.; Herbschleb, E. D.; Doi, Y.; Morishita, H.; Fujiwara, M.; Hatano, M.; Yamasaki, S.; Mizuochi, N. Engineering of Fermi Level by nin Diamond Junction for Control of Charge States of NV Centers. *Appl. Phys. Lett.* **2018**, *112*, 111903.
(42) Chavarría, C. C.; Payan, S.; Salvetat, J.-P.; Maglione, M.; Klein, A. Fermi Level Engineering for Large Permittivity in $BaTiO_3$-Based Multilayers. *Surfaces* **2020**, *3*, 567−578.

https://doi.org/10.1021/acsenergylett.3c02348
ACS Energy Lett. 2024, 9, 153−158